REPORT NO.
UCB/SEMM-90/22

STRUCTURAL ENGINEERING
MECHANICS AND MATERIALS

ANALYTICAL AND EMPIRICAL MODELS OF AXIAL FORCE DISPLACEMENT BEHAVIOR OF STEEL DOUBLE ANGLES

by

MARIO DE STEFANO
and
ABOLHASSAN ASTANEH

DECEMBER 1990

DEPARTMENT OF CIVIL ENGINEERING
UNIVERSITY OF CALIFORNIA
BERKELEY, CALIFORNIA

UNIVERSITY OF CALIFORNIA, BERKELEY

BERKELEY • DAVIS • IRVINE • LOS ANGELES • RIVERSIDE • SAN DIEGO • SAN FRANCISCO

SANTA BARBARA • SANTA CRUZ

CIVIL ENGINEERING

BERKELEY, CALIFORNIA 94720

Happy New Year

December 19, 1990

Nestor Iwankiw
Director, Research and Codes
AISC
One East Wacker Dr.
Suite 3100
Chicago, IL 60601-2001

Subject: Research on Double Angles Subjected to axial and shear loads.

Dear Nestor:

Enclosed please find a copy of a report on double angles subjected to axial load. This report is an outcrop of our main research project on behavior and design of double angles subjected to shear and axial loads. On that project we have completed the study and my student has submitted her thesis on that. Now I am working on developing design recommendations and procedures that can be used by designers in handling combined axial load and shear. I think I will have the final report on the project to you early in 1991 as promised.

Thank you for your support of our research activities.

Sincerely yours,

Hassan Astaneh

cc: R. O. Disque

ANALYTICAL AND EMPIRICAL MODELS OF AXIAL FORCE DISPLACEMENT BEHAVIOR OF STEEL DOUBLE ANGLES

by

Mario De Stefano, Graduate Research Assistant

and

Abolhassan Astaneh, Associate Professor

December 1990

Structural Engineering, Mechanics and Materials
Department of Civil Engineering
University of California
Berkeley, California

ANALYTICAL AND EMPIRICAL MODELS OF AXIAL FORCE DISPLACEMENT BEHAVIOR OF STEEL DOUBLE ANGLES

M. De Stefano and A. Astaneh

ABSTRACT

In recent years, the moment-rotation response of double angle shear connections has been deeply examined. However, the response of these connections to applied axial force has not been studied so extensively. This paper presents two mathematical models of the behavior of double angle shear connections subjected to axial load. The proposed axial force-axial displacement models are based on physical behavior of test specimens that were subjected to axial force until failure.

ACKNOWLEDGMENTS

The research reported herein was part of graduate research of the first author for his Master of Science degree. The authors wish to express their thanks to Professor Graham Powell of University of California at Berkeley for his valuable comments. The experimental tests were done by K.M. Mc Mullin and A. Astaneh at the University of Oklahoma, Norman, in 1985. The support of Department of Civil Engineering of the University of Oklahoma is sincerely appreciated.

This study was in part supported by the American Institute of Steel Construction, the University of California at Berkeley and by the California Department of Transportation (Caltrans) through the project: "Seismic Condition Assessment of the Bay Bridge" for which A. Astaneh is Principal Investigator.

TABLE OF CONTENTS

LIST OF FIGURES

SECTION 1

PHYSICAL BEHAVIOR OF DOUBLE ANGLE CONNECTIONS

The double angle connections that are examined in this paper were welded to the column and bolted to the beam as shown in Fig.1a. When a traction force $2F$ is applied to the beam, the force is transferred to the angles through the bolts. The force is eventually transferred to the column through the weld lines (Fig.1b). In a double angle connection, due to the symmetry, it is assumed that both angles behave in a similar manner as well as that a tension force F acts on each angle.

The behavior of double angle connections subjected to axial load, as shown in Figure 1b, can be summarized as follows[4,5]. In the initial elastic stage the outstanding leg of the angle is mainly subjected to bending while the back-to-back leg is subjected to axial force. As the axial tension force $2F$ and the displacement δ increase, the angle experiences inelasticity and cylindrical plastic hinges form at the end of the outstanding leg, first at the weld line and then adjacent to the fillet while the back-to-back leg remains almost elastic (Fig.2a). As the loading continues, the beam and back-to-back legs are continuously pulled away from the column and displacement δ increases. Gradually, the displacement becomes significantly large and outstanding leg develops significant membrane forces that no longer can be ignored. In addition, due to development of large rotations at the hinges, strain hardening of material causes increase in capacity of plastic hinges. Therefore, major behavioral characteristics are development of hinges in outstanding leg, significant kinematic hardening and strain hardening of outstanding leg and axial deformation of back-to-back leg. Eventually, as load increases, the deformed shape of angles tends to appear as shown in Fig.2b.

SECTION 2

ANALYTICAL MODEL OF A DOUBLE ANGLE SEGMENT

In development of analytical model the following assumptions are made[6,7]:

1) the plane sections of the beam web remain plane;

2) the double angle connection can be divided into segments of length *a* which act independent of each other (Fig.1a);

3) the shear on the connection is not very large, thus it does not affect the tension and compression properties of the angle segments.

Based on the above assumptions, the connection can be modelled with a parallel springs system as represented in Fig.1c[2,3,7]. Therefore, the analysis and modeling of one segment will be sufficient to define the overall behavior.

In the following, due to the dominant axial-bending action, the double angle segment is considered to be made of inelastic beam elements, while the steel constitutive relationship σ - ε is assumed to be bilinear elastic strain-hardening (Fig.3). Using the bilinear σ - ε model, stress distribution across the cross section will be as shown in Fig.4b.

First, let us examine the flexural behavior as well as the stiffening effect due to membrane force of the outstanding leg. The moment (M) - curvature (χ) relationship for the generic section of the outstanding leg is given by:

$$M = EI\chi \tag{1}$$

in the elastic stage and

$$M = \frac{2}{3}\sigma_y a t_y^2 + 2a\left\{\frac{\sigma_y}{2}\left[\left(\frac{t}{2}\right)^2 - \left(\frac{\varepsilon_y}{\chi}\right)^2\right] + E_2\frac{\chi}{3}\left[\left(\frac{t}{2}\right)^3 - \left(\frac{\varepsilon_y}{\chi}\right)^3\right] - E_2\frac{\varepsilon_y}{2}\left[\left(\frac{t}{2}\right)^2 - \left(\frac{\varepsilon_y}{\chi}\right)^2\right]\right\} \tag{2}$$

in the strain-hardening stage, where a, t, t_y are represented in Fig.4c and I is the inertia moment of cross section of the outstanding leg.

As shown in Fig.5 modeling the end restraints of such a beam is very complex. In fact, a realistic boundary condition should be represented by rotational and translational springs whose stiffness terms $k_{A\varphi}$, $k_{B\varphi}$ and k_{Bt} are not constant and difficult to determine. However, in this study the beam is assumed to be clamped at both ends developing fixed boundaries, as shown in Fig.6a. This is an approximation due to the fact that the welded end A as well as point B and C are not perfectly fixed and can rotate, as shown in Fig.6b. Then, due to this approximation, the initial elastic stiffness of the model is expected to be larger than the actual elastic stiffness.

If the leg segment is subjected to pure bending, since the system is antisymmetric, the relationship between the applied force F and the resulting displacement δ can be obtained by solving the compatibility equation (3) on the rotation Φ_B at the end B (Fig.7a):

$$\phi_B = \phi_{BM} + \phi_{B\delta} = 0 \tag{3}$$

where Φ_{BM} is the rotation at point B due to the end moments M (Fig.7c) and $\Phi_{B\delta}$ is the rigid body rotation due to the imposed displacement δ.

To obtain Φ_{BM} it is possible to apply the principle of virtual force considering a virtual unit load condition which gives the moment distribution M' (Fig.7b) and considering the curvature distribution χ_M, due to the end moments M, as the deformation field (Fig.7c).

Then, the rotation Φ_{BM} can be obtained from:

$$\phi_{BM} = \int_0^L M' \chi_M dx \tag{4}$$

and finally:

$$\delta = -L\phi_{BM} \tag{5}$$

Since the moment M is related to the force F through the relationship:

$$F = \frac{2M}{L} \tag{6}$$

then Equation (5) defines the F - δ relationship.

The above derivation is a first order inelastic analysis, which does not account for the geometric stiffening and development of membrane force in outstanding leg. In the following, an approximate procedure is presented to compute the axial force N and to evaluate its effect on force - displacement response of double angle segments.

The axial force N developed in outstanding leg is transmitted from the back-to-back leg, in which it acts as shear (Fig.8a). If it is assumed that the node B cannot rotate, the incremental compatibility equation which is needed to compute the increment dN can be written as:

$$-de + (dN)(f_{at})_h = (dN)(f_{st})_v \tag{7}$$

In Equation (7) de is the increment of the axial shortening of the outstanding leg in the absence of axial force due to a displacement increment $d\delta$, dN is the correspondent increment of axial force, $(f_{at})_h$ is the tangent axial flexibility of outstanding leg and $(f_{st})_v$ is the tangent shear flexibility of the back-to-back leg.

To calculate de, a second order analysis is needed. For the beam A-B (Fig.7a) the elastic shape function which relates the nodal displacement δ with the transversal displacement function $w(x)$ is given by:

$$w(x) = \left[\frac{3}{L^2}x^2 - \frac{2}{L^3}x^3\right]\delta \tag{8}$$

A second order approximation of the axial shortening can be obtained from:

$$de = \frac{1}{2}\int_0^L w'^2(x)dx = \frac{3}{5L}(d\delta)^2 \tag{9}$$

This is the quadratic relationship which relates the displacement increment $d\delta$ with the shortening increment de in the elastic range (Fig.8b). In the following, it is assumed that this relationship still holds in the inelastic field. In other words, the shape function (8) is considered valid even in the post-elastic stage.

The tangent axial flexibility $(f_{at})_h$ is the operator which relates the axial displacement increment dq with the normal force increment dN through the equation:

$$dq = (f_{at})_h dN \tag{10}$$

which can be also written as:

$$dN = (k_{at})_h dq \tag{11}$$

where $(k_{at})_h$ is the tangent axial stiffness of outstanding leg. Assuming the usual extensional shape function:

$$u(x) = \frac{x}{L} q \tag{12}$$

and assuming that it also holds in the inelastic range, the extensional deformation ε is given by:

$$\varepsilon = \frac{1}{L} q = Bq \tag{13}$$

and the extensional tangent stiffness is given by:

$$(k_{at})_h = \int_0^L B\,[EA_t(x)]B\,dx \tag{14}$$

where $EA_t(x)$ is the tangent axial stiffness which varies along the beam.

To obtain an approximate value of $EA_t(x)$ the flexural problem is solved independent of the extensional one. Moreover, when the i-th displacement increment $d\delta$ is given, the tangent stiffness of the (i-1)th step is introduced in the compatibility Equation (7) without iterating to define its exact value at i-th step.

Once the compatibility equation at i-th iteration is solved , the value of dN is known and by using Equations (10) and (13) the increment of extensional deformation is found. In this manner the curvature χ_i and the centroidal axial deformation ε_i are computed section by section. By dividing the generic section into strips and assuming that the plane cross sections remain plane, it is possible to calculate the deformation $\varepsilon_{i,j}$ for each strip j at step i by using:

$$\varepsilon_{i,j} = -\chi_i y_j + \varepsilon_i \tag{15}$$

where y_j is the distance from the centroid of the section to the centroid of the j-th strip. By using the correspondent elasticity modulus, E_j, the axial tangent stiffness is numerically evaluated by:

$$EA_i(x) = \sum_{j=1}^{n} E_j A_j \tag{16}$$

where A_j is the area of the j-th strip. Notice that the stiffness $EA_i(x)$ is used in the (i+1)-th step.

The tangent shear flexibility $(f_{si})_v$ is also obtained by an approximate procedure. In fact, the back-to-back segment is modelled as a clamped beam, without taking into account the rotations of nodes B and C (Fig.6a). Moreover at the i-th step the previous (i-1)th value of $(f_{si})_v$ is used. The solution of the Equation (7) results in obtaining the increment of the transversal displacement of vertical segment, δ_v, as well as the increment of the shear, which is equal to dN to satisfy equilibrium of node B. Then the value of tangent flexibility used in the (i+1)th step is:

$$(f_{si})_{v,i+1} = \frac{dN_i}{d\delta_{v,i}} \tag{17}$$

Therefore, at the i-th step only the value of dN_i in Equation (7) is unknown and its determination leads to obtaining value of the axial force N_i as:

$$N_i = N_{i-1} + dN_i \tag{18}$$

The stiffening effect of the axial membrane force can be evaluated by the simplified formula:

$$F_{IIord} = F_{Iord} + \frac{N_i \delta_i}{L} \tag{19}$$

where $F_{I\,ord}$ is the first order tension force value computed by equations (5) and (6) and $F_{II\,ord}$ is the second order tension force that includes effect of the membrane force.

The above procedure allows the computation of the relationship between force F and displacement δ with two types of assumptions. The assumptions made to determine the flexibility coefficients $(f_{si})_h$ and $(f_{si})_v$ affect the results based on the size of the displacement increment $d\delta$ in the following manner : the smaller is $d\delta$, the more accurate is the approximate solution. The kinematic hypotheses affect the calculations more deeply, especially the end restraint conditions influence the results significantly. In fact, the assumption of clamped end conditions results in the calculated initial stiffnesses to be larger than the values obtained from the experiments.

SECTION 3

EXPERIMENTAL DATA AVAILABLE

To study axial response of double angle connections, four tests were conducted in 1985 by K. Mc Mullin and A. Astaneh. The experimental set-up was for all four tests the same and is shown in Fig.9, while the properties of the specimens are given in Table I.

Table I. Properties of test specimens.

	Double angle	Steel	Weld length	Weld size	Electrode
Test A1	4 x 3-1/2 x 3/8 (in)	A36*	3.0 (in)	1/4 (in)	E70xx**
Test A2	5 x 3-1/2 x 5/8 (in)	A36*	3.0 (in)	9/16 (in)	E70xx**
Test A3	4 x 3-1/2 x 1/2 (in)	A36*	3.0 (in)	7/16 (in)	E70xx**
Test A4	4 x 3-1/2 x 3/8 (in)	A36*	3.0 (in)	5/16 (in)	E70xx**

Note :
1 in = 25.4 mm
* A36 steel has f_y = 36 ksi (248 MPa) and f_u = 58 ksi (400 MPa)
** E70xx electrode has a strength of 70 ksi (483 Mpa)

The results of experiments are presented in terms of axial force $2F$ versus axial displacement δ. Those plots are given in Fig. 10.

The experimental $2F$ - δ curves showed three distinct phases. The first phase was mainly elastic, the second phase was inelastic - strain hardening and the third phase was a " geometric " hardening apparently due to development of significant membrane forces. In fact, after an initial elastic behavior, the specimens began to show yielding along the weld with formation of a plastic

hinge in the weld throat. Thereafter, significant yielding appeared on the angle adjacent to the fillet corner and a second plastic hinge formed there. Further incremental application of force $2F$ were resisted mainly by membrane actions developed in the outstanding legs of angles.

A comparison between the experimental data and the proposed analytical model is presented in the following section.

SECTION 4

COMPARISON OF EXPERIMENTAL RESULTS AND ANALYTICAL MODEL

In Fig.10 the experimental $2F$ - δ relationships are compared to the analytical predictions. Two analytical models are represented; the first one predicts smaller values of force $2F$ for a given displacement and is obtained without considering the second order stiffening effect due to axial force. The second curve gives larger force values than the first model for the same displacement and is obtained by using Equation (19), which includes membrane forces. In the elastic range both analytical models are virtually coincident. In the inelastic phase, the first analytical model always shows a decreasing stiffness whereas the second curve presents an increasing stiffness, when the displacements become very large.

In particular, as expected, both analytical models present an initial stiffness k_1 given by :

$$k_1 = 2\frac{12E_1I}{L_o^3} \tag{20}$$

and the slope of those obtained without considering the axial force effect tends to the limit value k_2 given by :

$$k_2 = 2\frac{12E_2I}{L_o^3} \tag{21}$$

The parameter L_o in the above equations not only affects computed stiffness but also it affects strength of the connection. Therefore, by changing L_o, the closeness of the analytical predictions to the available test results was studied. It was found that, by choosing L_o to be equal to overall width of outstanding leg, the analytical results fitted the experimental results better.

In order to include material strain-hardening, a bilinear σ - ε relationship was used. The value of strain hardening modulus E_2 was selected to be 750 ksi (5170 MPa). It must be realized that value of strain-hardening modulus is less certain than the elastic modulus. The above value for E_2 is the average of results from four tests.

In particular, the tests A1 and A4 are simulated with the same model, since they only differ in the weld size D, which does not influence the model. By taking into account second order effects, the force values predicted by analytical model are greater than the experimental values for test A1 and are smaller for test A4. This is explained by the fact that Specimen A1 had weld size smaller than Specimen A4 . As a result, the strength of Specimen A1 was smaller than Specimen A4.

The force-displacement relationship of test A2 seems to be simulated by the two analytical curves with the same degree of accuracy. For this test the experimental values are intermediate between the two analytical models. However, it should be noticed that the curve corresponding to the model taking into account the geometric effect better approximates the shape of the inelastic branch of the test results. By varying E_2 this model appears to have the potential of giving better results.

Test A3 is characterized by less stiffening influence of N, which means that the shape of both analytical curves are not as closely representing the test results as for the previously discussed tests.

In conclusion, the comparison between experimental and analytical curves shows that they mainly differ in the initial elastic stage. In fact , as expected, the initial stiffness of the experimental curves is much lower than the analytical ones. On the other hand, there is a good agreement in the inelastic stage, both in terms of strength and stiffness. Particularly, the effects of material and kinematic hardening are realistically represented in the models.

SECTION 5

FORMULATION OF A PROPER EMPIRICAL MODEL.

As mentioned earlier, all the experimental curves show an initial elastic behavior, a subsequent inelastic-strain hardening behavior and a final kinematic hardening. Since there are three distinct phases of behavior, it is logical to use a single tri-linear empirical model to represent these three stages of behavior. A tri-linear model of force-displacement response can be defined by six parameters, k_1, $(2F)_y$, k_2, δ',δ'' and ΔF, as shown in Fig.11, where k_1 is the initial stiffness, $(2F)_y$ is the conventional force limit, which separates the elastic stage from the inelastic, k_2 is the slope of strain-hardening branch, δ' is the displacement value which defines the beginning of significant second-order effects, δ'' is the ultimate displacement and ΔF is the expected increment of the strength primarily due to the geometric effects.

The results previously obtained seem suggest that a propped cantilever beam is a more convenient model to represent outstanding leg of the angles during initial elastic phase of behavior. In fact, the experimental observations reveal that the welded end is subjected to significant rotations during the loading. Therefore, the value of the initial stiffness k_1 is given by:

$$k_1 = 2\frac{3EI}{(L_o - f)^3} \tag{22}$$

where L_o is the full length of the outstanding leg and f is the fillet size, as shown in Fig.12. The values of k_1 provided by Equation (22) match well the average initial stiffness values of the experimental curves (see comparison of Table II).

The value of $(2F)_y$ depends on the strength of both the welded end and the fillet end and can be evaluated by this expression :

$$2F_y = 2\frac{(M_{pw} + M_{pb})}{(L_o - f)} \tag{23}$$

where M_{pw} is the ultimate plastic moment of the weld and M_{Pb} is the ultimate plastic moment of the outstanding leg. Values of M_{pw} and M_{Pb} are given by:

$$M_{pw} = \sigma_{uw}\frac{a}{4}\left(\frac{D}{\sqrt{2}}\right)^2 \tag{24}$$

$$M_{pb} = \sigma_u a\frac{t^2}{4} \tag{25}$$

The values of σ_{uw} and σ_u are selected by increasing the conventional nominal yield values a factor of *5/3*. This factor is selected to approximate ratio of σ_u/σ_y for constructional steel. Then, the following values were introduced in Equations (24) and (25):

$\sigma_{uw} = 70\ ksi \quad (489\ MPa)$

$\sigma_u = 60\ ksi \quad (414\ MPa)$

The values of $(2F)_y$ for the examined cases are reported in Table II.

The parameter k_2 represents the stiffness of the strain-hardening branch; in the analytical model, the slope k_2 decreases as displacement δ increases and, in absence of the second order effects, it asymptotically tends to:

$$k_2^1 = \frac{E_2}{E_1}k_1 \tag{26}$$

Thus, the value of k_2 to be introduced in the tri-linear model must be larger than k_2^1, but it seems reasonable to relate k_2 with this limit value : in Table II the values of k_2 given by:

$$k_2 = 3\left(\frac{E_2}{E_1}\right)k_1 \tag{27}$$

are reported. With this values the tri-linear force $2F$ - displacement δ relationships showed in Fig.12 were obtained.

The values of ΔF were determined assuming that during the load history the back-to-back leg essentially remains in the elastic range. This assumption is supported by the experimental observation and is also confirmed by the analytical results. Following this hypothesis, the maximum shear developed in the back-to-back leg, which is equal to the maximum axial membrane force in the outstanding leg, is given by:

$$S_y = \frac{2M_y}{L_b - f} \tag{28}$$

where:

$$M_y = \frac{2\sigma_y I}{t} \tag{29}$$

In Equation (28) M_y is the yielding moment and L_b is the distance between the bolt center and the angle corner. Then the increment of the force $2F$ due to membrane behavior can be given by:

$$\Delta F = 2\frac{S_y \delta''}{L_o - f} \tag{30}$$

In Table II the experimental values of ΔF are compared with the empirical ones provided by Equation (30).

Further studies are needed to compute in a proper way the parameters δ' and δ''. In this paper the experimental values were used in order to define the trilinear empirical law (Table II).

The curves presented in Fig.13 seem to fit the experimental data reasonably well.

Table II. Parameters established for the empirical model.

	TEST A1	TEST A2	TEST A3	TEST A4
k_1 (kips/in) EXPERIMENTAL	60.60	155.96	158.31	70.07
k_1 (kips/in) ANALYTICAL	143.37	339.84	339.84	143.37
k_1 (kips/in) EMPIRICAL	70.84	182.52	189.30	70.84
$(2F)_y$ (kips) EMPIRICAL	5.00	13.36	10.63	5.58
k_2 (kips/in) EMPIRICAL	6.39	16.44	17.04	6.39
ΔF (kips) EMPIRICAL	1.84	6.22	2.48	1.84
ΔF (kips) EXPERIMENTAL	1.90	5.74	2.48	1.94
δ' (in) EXPERIMENTAL	0.379	0.438	0.316	0.399
δ''(in) EXPERIMENTAL	0.687	0.750	0.495	0.477

Note :
1 in = 25.4 mm
1 kip = 4.449 kN
1 kip/in = 0.1752 kN/mm

SECTION 6

CONCLUSIONS

In this paper the experimental results of four tests on angle segments subjected to monotonic tension were studied in order to improve understanding of physical behavior and to propose a simplified way to define an empirical force - displacement relationship.

The results given by an analytical model well approximated the experimental results and gave useful information in order to evaluate the stiffness and strength parameters, which are needed to build the empirical constitutive law.

Further studies are necessary to determine the failure of the angle segment or its connectors. For angle failure, this could be done by introducing a proper limit state criterion in terms of interaction of moment M and axial force N acting on the cross sections of the outstanding leg.

REFERENCES

1) Astaneh-Asl, A., Nader, M.N., And Malik, L. "Cyclic Behaviour of Double Angle Connections", Journal of Structural Engineering, ASCE, vol. 115, No. 5, Paper No. 23469, May 1989.

2) Azizinamini A., Radziminiski James R., "Static and Cyclic Performance of Semirigid Steel Beam-to-Column Connections", Journal of Structural Engineering, ASCE, vol.115, December 1989.

3) Harper, W.L., Dickerson, J.R., Bradburn J.H., And Radziminski, J.B. " Static and Cyclic Behavior of Semi-Rigid Bolted and Welded Beam-Column Connections", Structural Research Studies, Department of Civil Engineering, University of South Carolina, Columbia, S.C., May 1990.

4) Ho, I. And Astaneh-Asl, A. "Behavior and Design of Double Angle Shear Connections Subjected to Axial Loads", UCB/EERC, University of California at Berkeley, Earthquake Engineering Research Center, 1990 (to appear).

5) Jain, A.K., Goel, S.C., And Hanson, R.D., "Hysteretic Cycles of Axially Loaded Steel Members", Journal of the Structural Division, ASCE, Vol. 106, No ST8, Proc. Paper 15607, August 1980.

6) Richard, R.M., Rabern, D.A., Hormby, D.E., And Williams, G.C., "Analytical Models for Steel Connections", Proceedings of the W.H. Munse Symposium, ASCE, May, 1983

7) Richard, R.M., Hsia, W.K., Chmielowiec, M., "Moment Rotation Curves for Double Framing Angles", Materials and Members Behaviour, Proceedings of the Sessions at Structures Congress '87, Orlando, Florida, 1987.

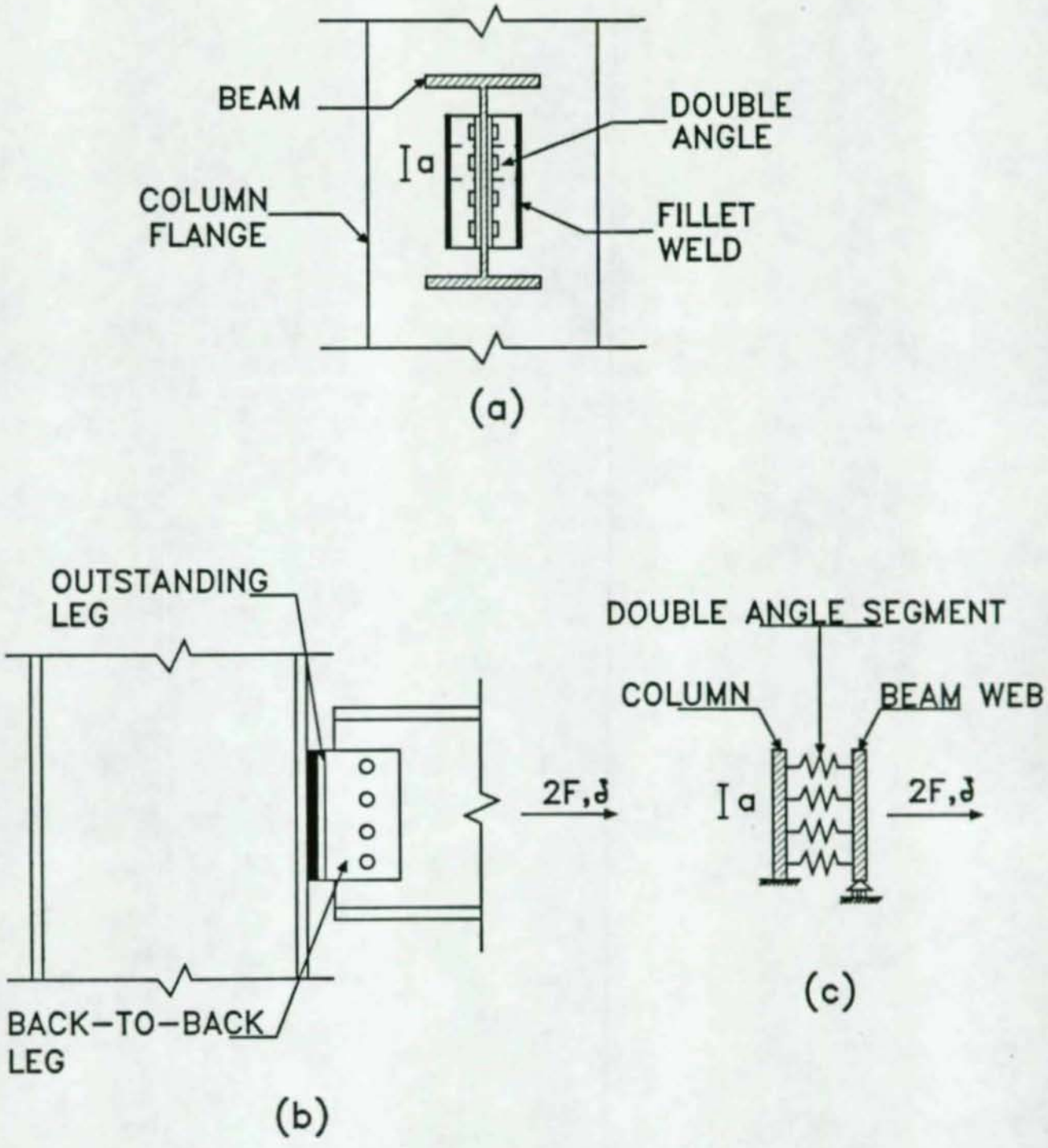

Fig.1. Double angle connection (a),(b) and analytical model (c).

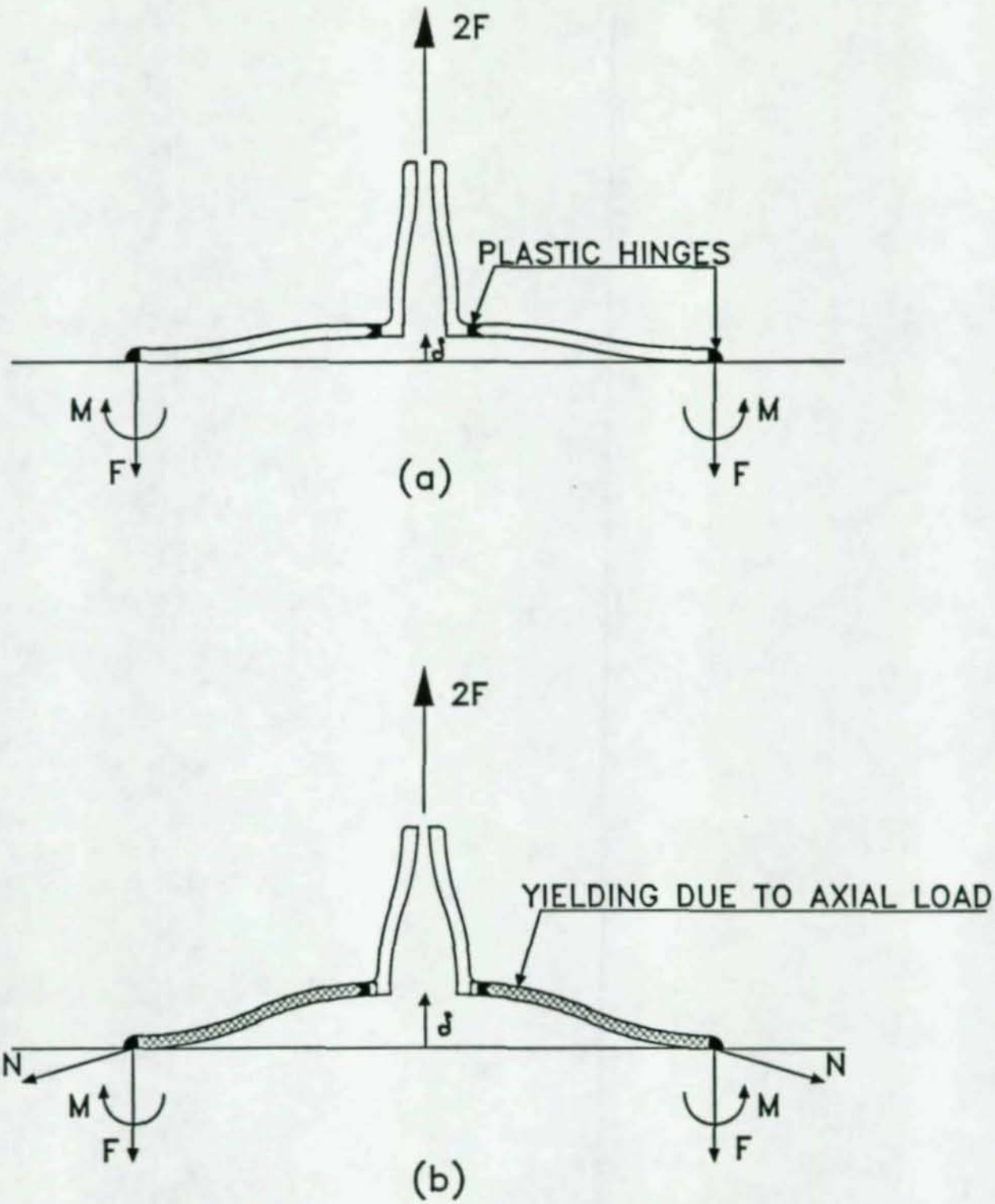

Fig.2. Behavior of double angle connection under tension loading.

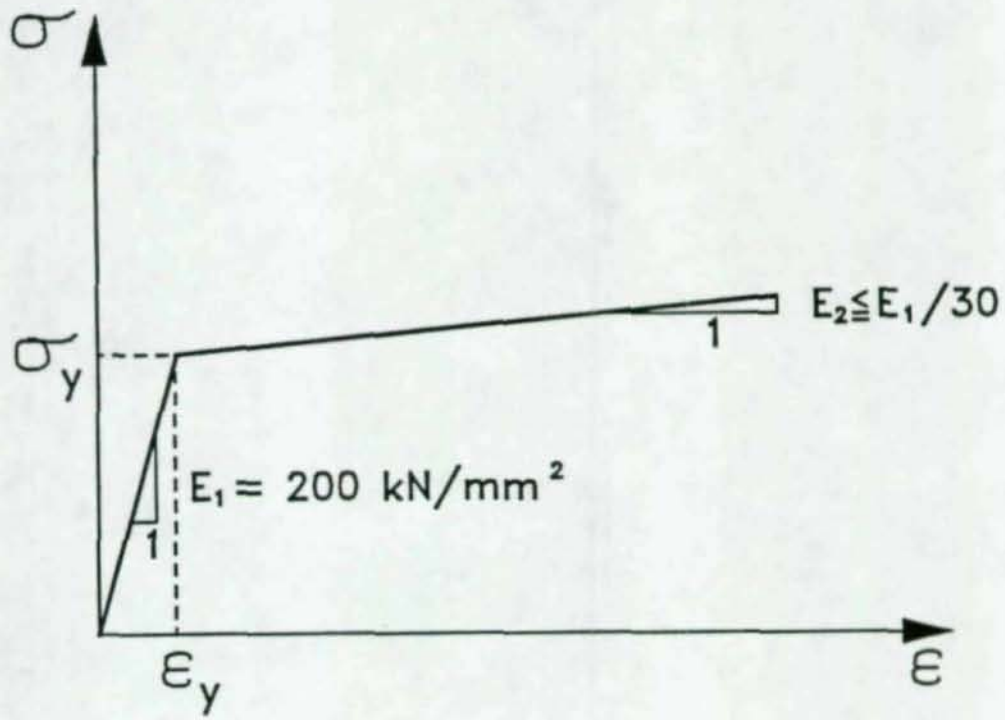

Fig.3. Steel bilinear constitutive relationship σ-ε.

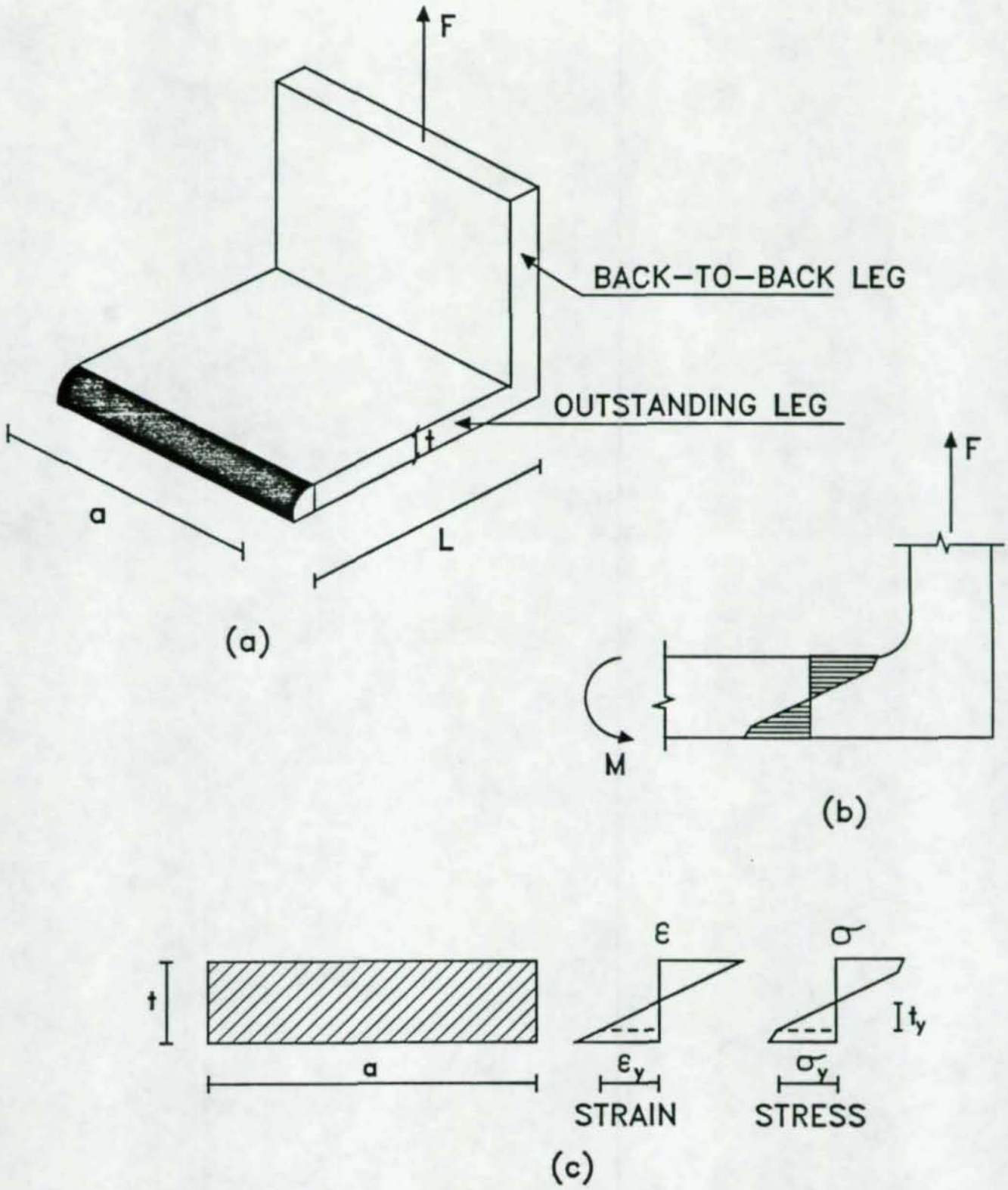

Fig.4. Stress and strain distribution on the cross section of outstanding leg.

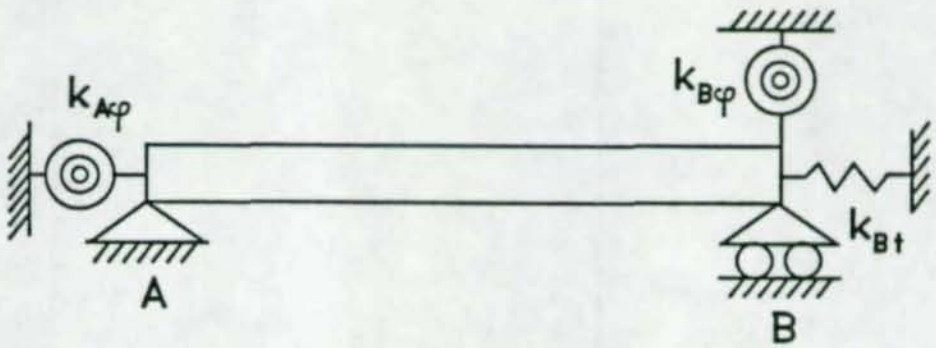

Fig.5. Actual end restraints for the beam segment A-B.

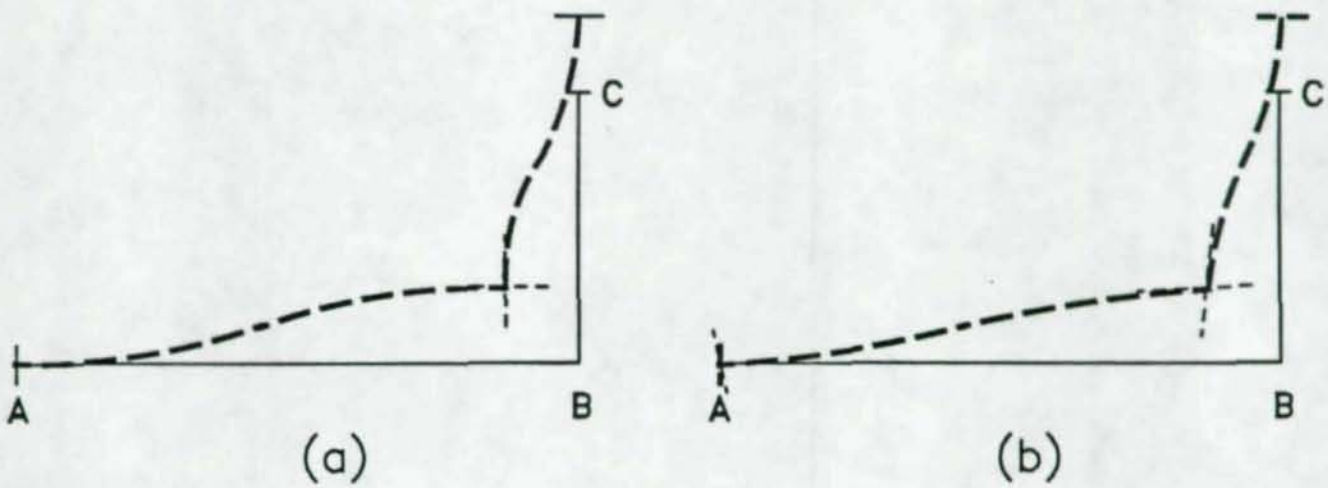

Fig.6. Assumed (a) and actual (b) deformed shape of angle under tension force.

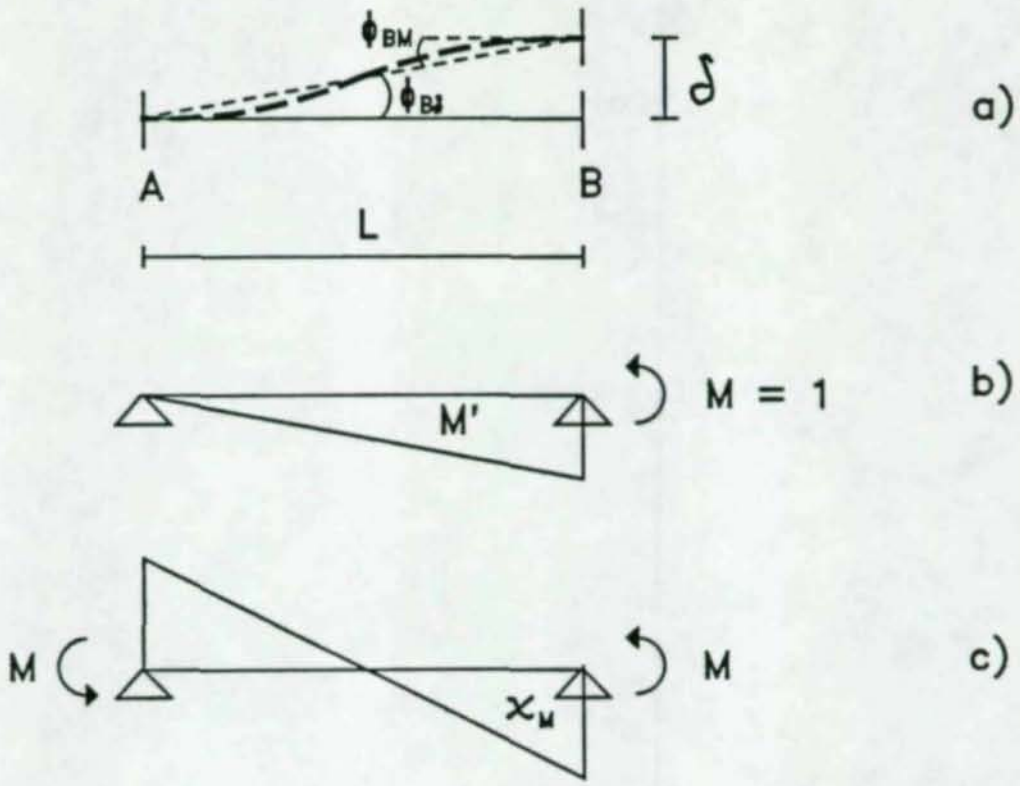

Fig.7. Schemes needed to apply the principle of virtual forces.

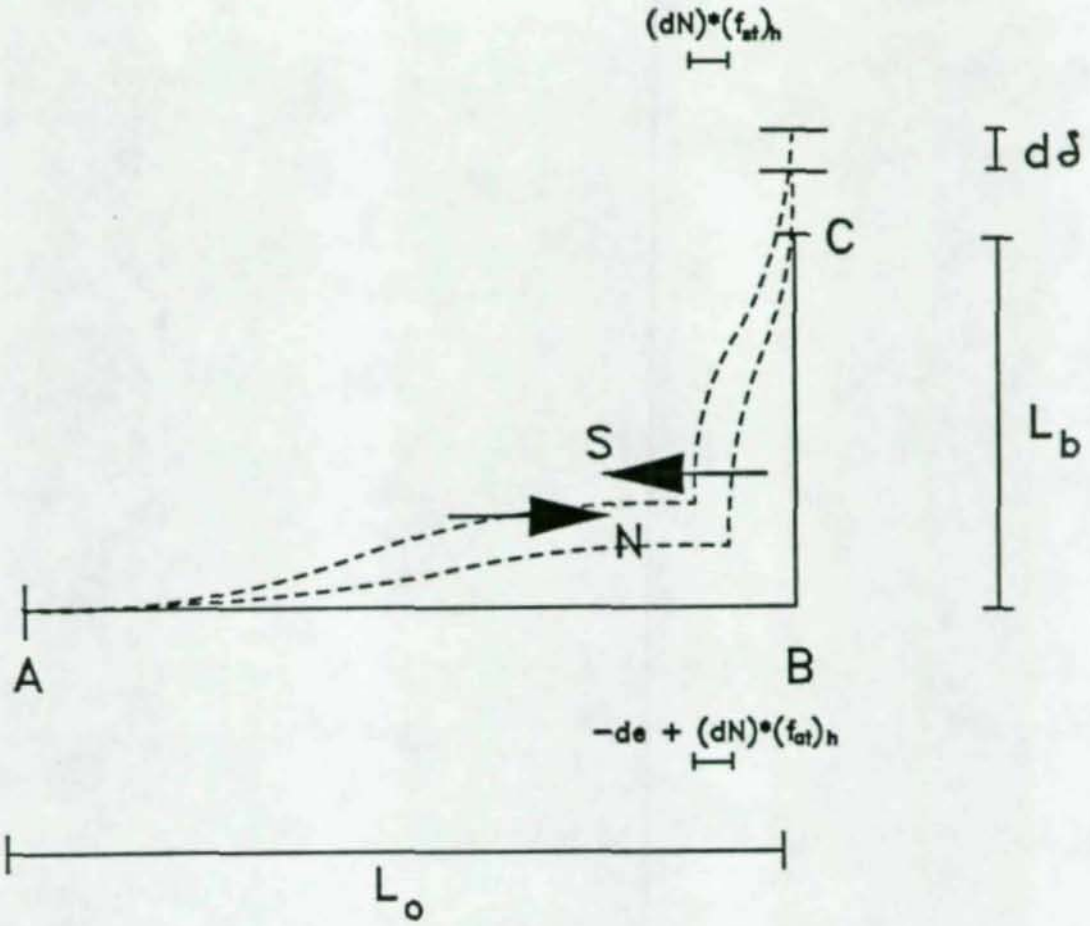

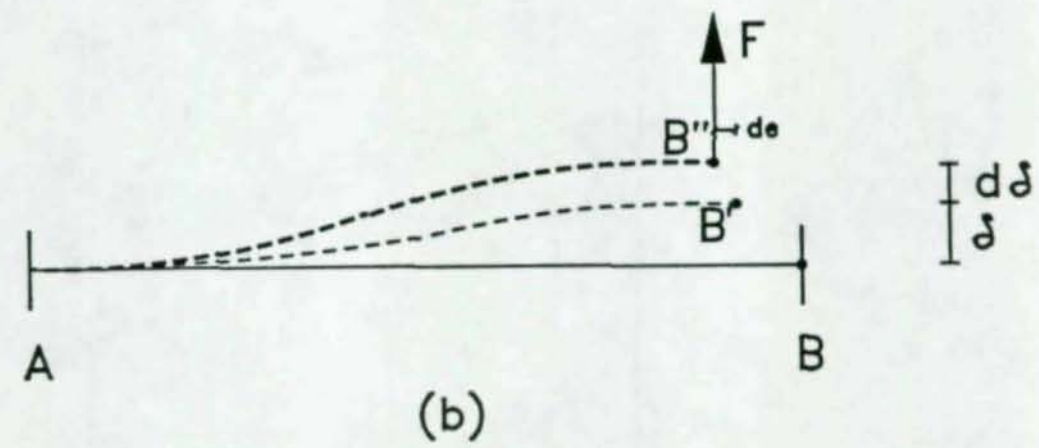

Fig.8. Description of the compatibility equation (7).

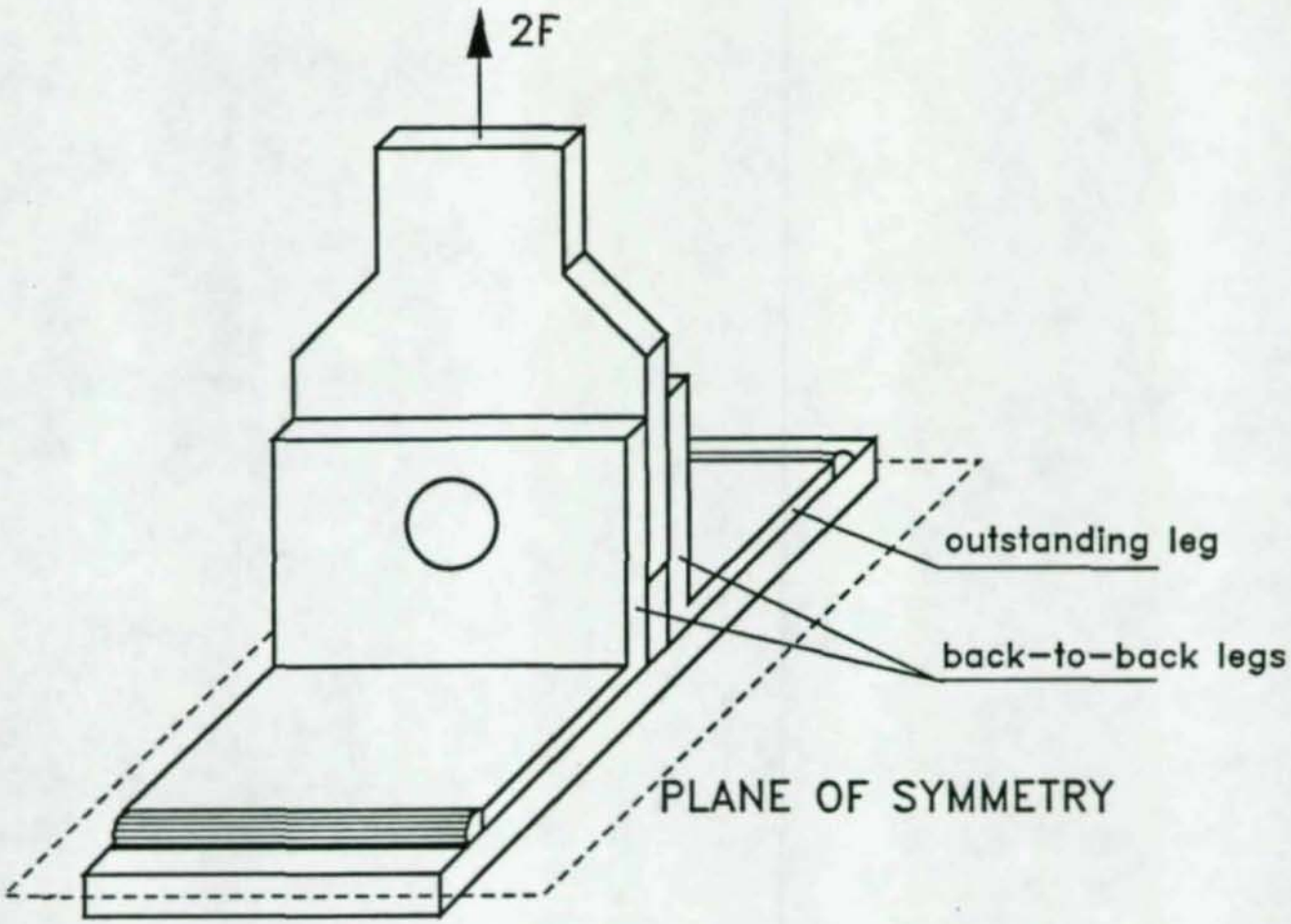

Fig.9. Experimental set-up used to determine the $2F$-δ relationship.

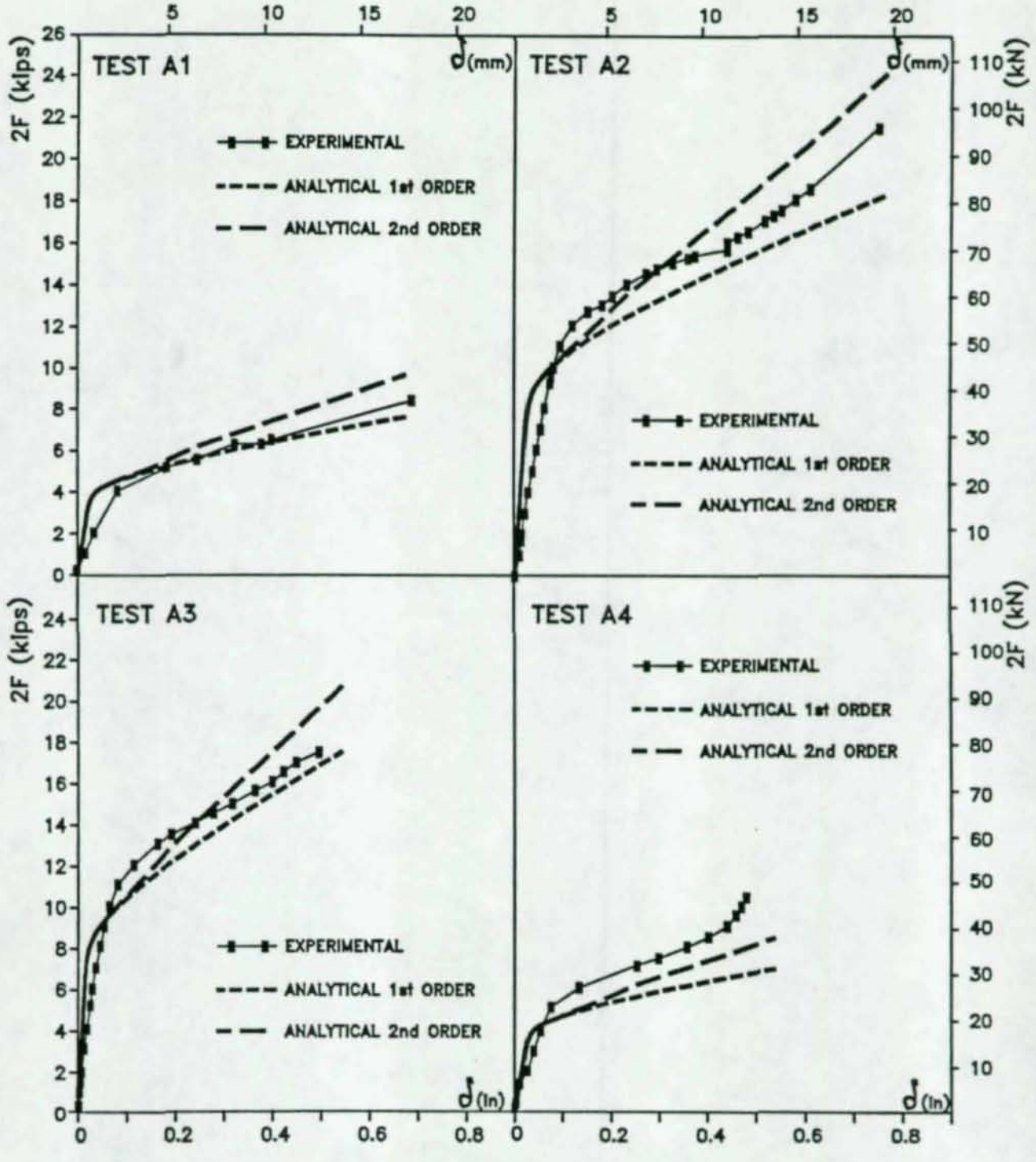

Fig.10. Comparison between analytical and experimental results.

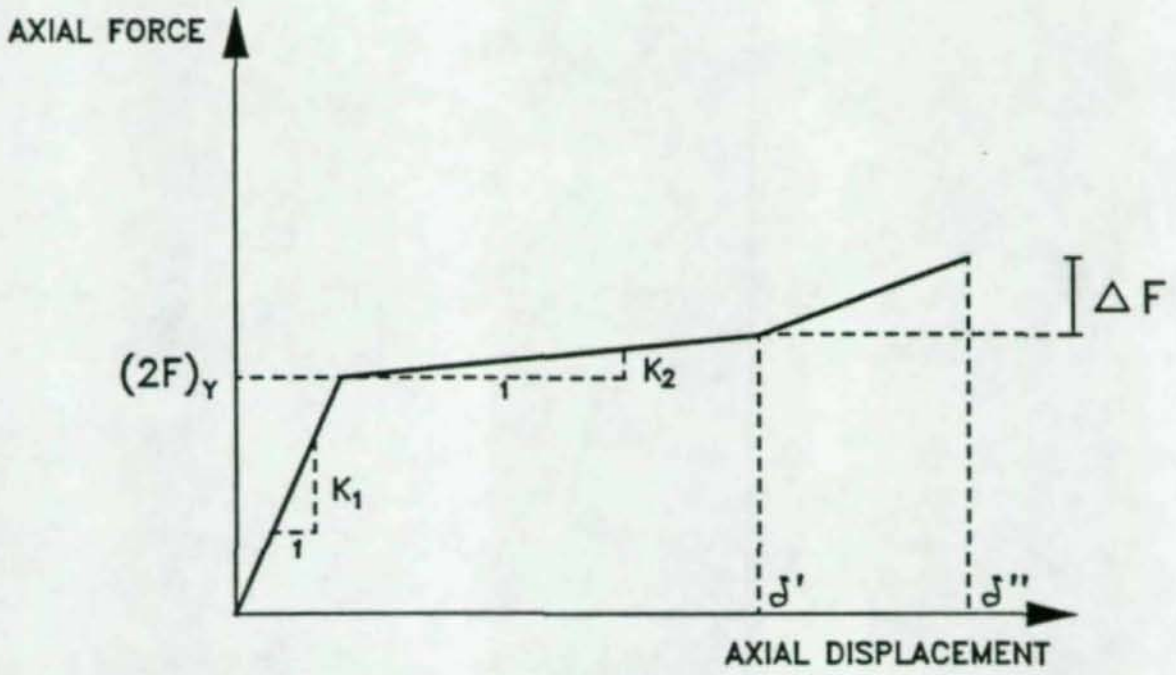

Fig.11. Parameters defining the trilinear empirical force-displacement relationship.

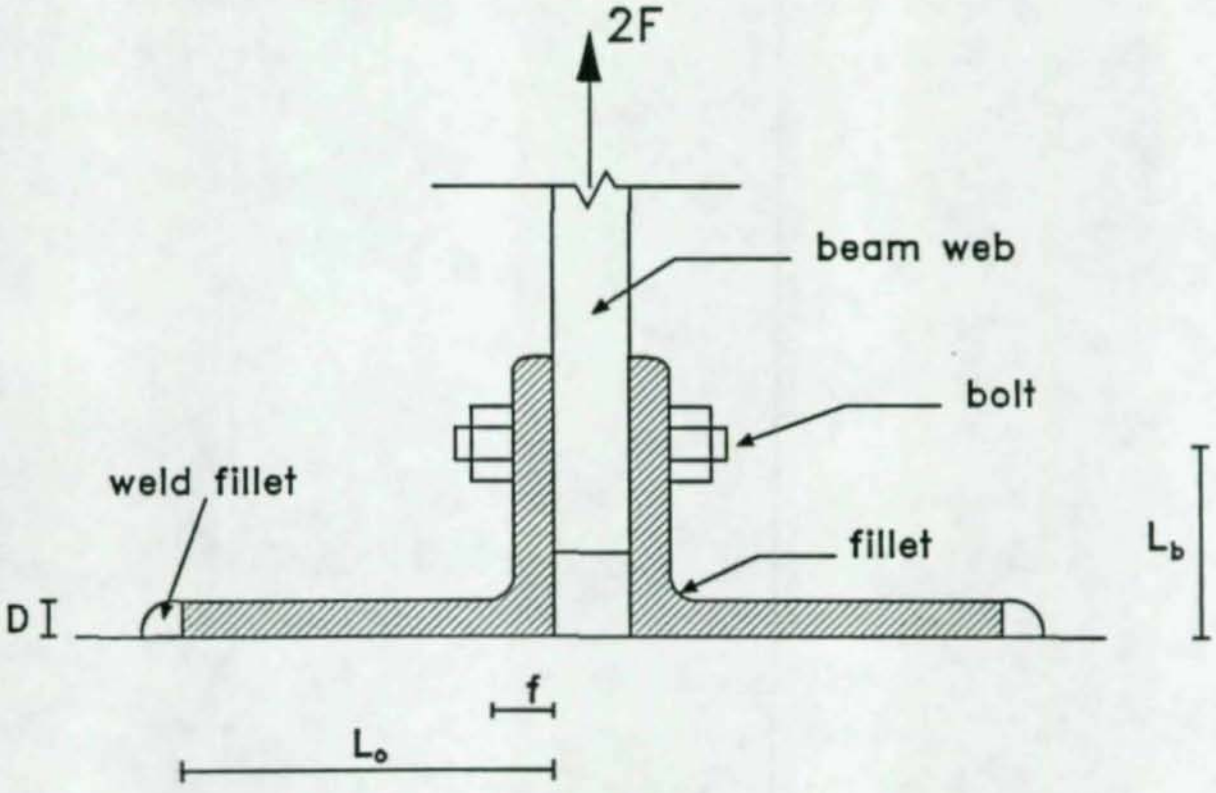

Fig.12. Cross section of a steel double angle connection.

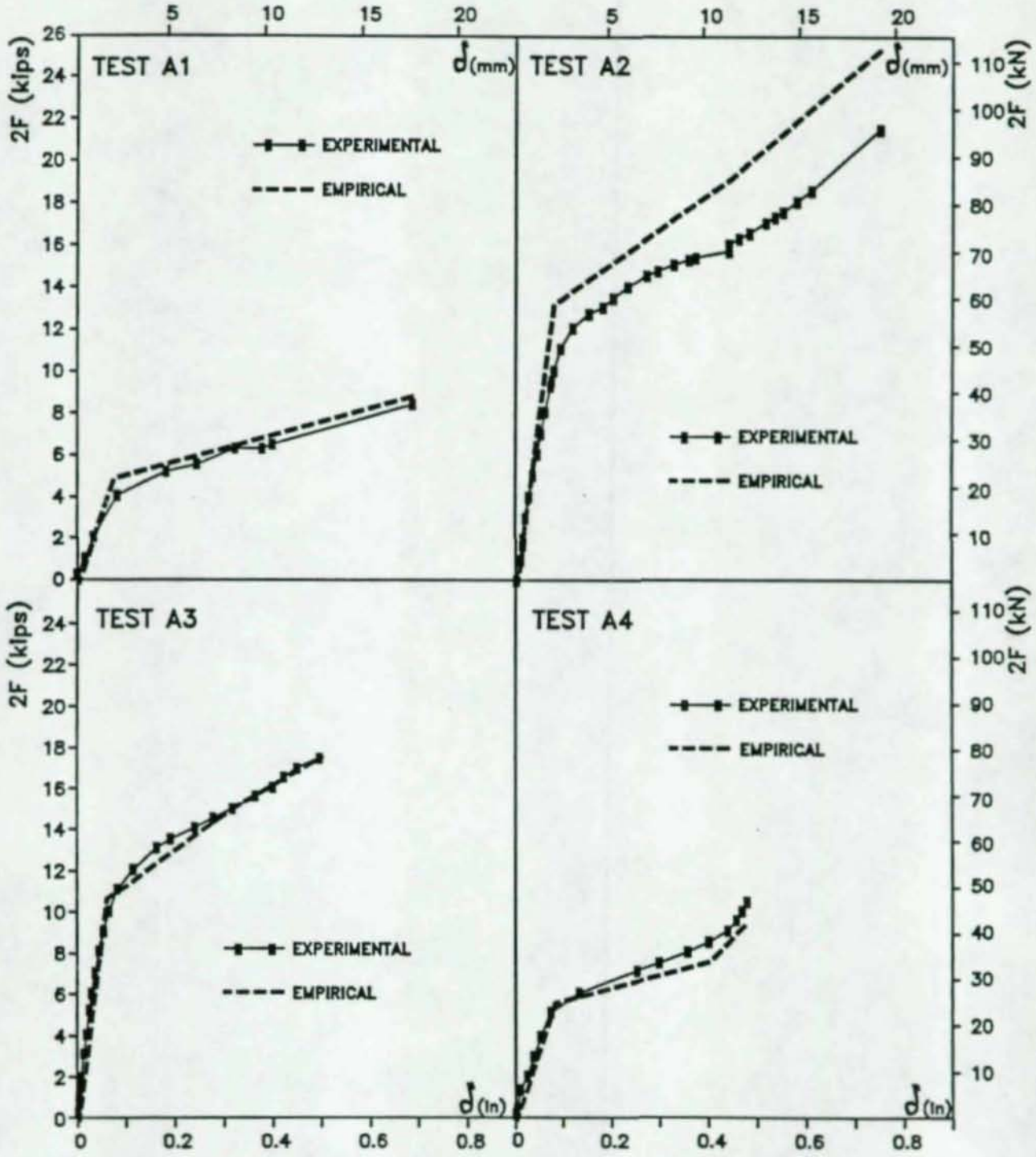

Fig.13. Comparison between empirical and experimental results.